

Experimental studies and finite element simulation of ultrasonic welding of Cu alloy

N. MOHAN RAJ^{1,2}, L.A. KUMARASWAMIDHAS² and S. ARUNGALAI VENDAN^{3*}

¹Department of Mechanical Engineering, Sri Krishna College of Technology, Coimbatore

²Department of Mining Machinery Engineering, Indian School of Mines, Dhanbad

³School of Electrical Engineering, VIT University, Vellore

Abstract. This research study aims to investigate the mechanical and metallographical aspects of ultrasonic welding of Cu-Cu wires. Experimental trials have been conducted and observations have been recorded as a database that collates parametric, quality and strength aspects of various weldments. Destructive testing and metallurgical characterizations have been carried out to examine the strength and integrity of the weldment. The key focus of this research attempt is laid on determining and evaluating the factors that governs the strength of the weldment. Metallurgical characterizations reveal vital information on the weld integrity and the extent of grain distribution. Further, FEM is employed to understand the deformation and thermal aspects involved in Cu-Cu welding using ultrasonics. The numerical model may provide an insight into the thermal phenomenon governing the joining process and subsequently estimation of the impact. Response surface methodology is employed to identify the parametric interdependencies and subsequently determine the optimized range.

Key words: ultrasonic, wire, Cu alloys, finite element method.

1. Introduction

Ultrasonic welding is employed for joining metals and its alloys with the application of high frequency ultrasonic vibrations. Welding of dissimilar materials is essential as it forms a configured structure for several product based industries. Available literatures emphasize the lacunas in joining of dissimilar materials and further record the possible causes for such observations. Considering the significance of this technical challenge posed by welding industry and its associates, an attempt is made in this research to evolve a solution to cater to their immediate requirements by employing ultrasonic welding. In specific the key objective has been framed with prominent weightage levied on joining Cu alloys. Ultrasonic welding of metals consists of complex processes such as breaking of contaminant films, fatigue crack information and propagation, fracture, generation of heat by friction. Ultrasonic welding technique can be employed to join dissimilar materials. In this research study, joining of dissimilar materials is becoming important to reduce weight and improve the performance of engineering structures. Some physical characteristics, namely melting temperature and coefficient of thermal expansion, may influence the process. Some of the important literature that provides greater insight into the concepts and research schemes pertaining to dissimilar welding that has contributed to this study are briefly discussed.

2. Literature review

Tsujino et al. [1] reported ultrasonic butt welding of thick metal plate specimens. Aluminium and copper plates with an average thickness of 6mm were used for the study. The significant parameter altering the weld strength was observed to the welding time while maintaining the pressure and corresponding vibration in a short variable range, the hardness also measured. A peculiar drop in the hardness adjacent to the weld surface was noted and it was addressed with a solution. The same authors [2] further investigated the properties of the ultrasonic weldments of thick metal plates with large capacity static induction thyristor. Compared to their previous study, there was a gradual increase in the hardness. Besides, the impact of the static clamping pressure on the weld strength while maintaining welding time and vibration amplitude constant was effectively studied. Added to this, the same authors [3] further carried out experimental studies on ultrasonic bonding of thin wires.

The main focus was on vibration frequency and its effect on weldment. The relationship between vibration velocity and welding strength were analysed. Subsequently, the interdependency of welding time and welding strength were examined. The vibrations were majorly classified into linear and complex types. Kim [4] evaluated the feasibility of ultrasonic bonding of hermetic micro electromechanical systems. The bonding patterns were investigated using SEM photographs. Moreover the various parametric analyses were also carried out for optimizing the range.

Tsujino et al. [5] presented a detailed study on dissimilar metal welding of aluminium to copper, aluminium to nickel,

*e-mail: arungalaivendan@vit.ac.in

and aluminium alloys for its application in fuel cells and hybrid automobiles. The welding characteristics and structural changes with respect to various parameters were investigated. The same authors [6] extrapolated their ideas to weld non-ferrous metals such as copper bimetallic strip, braided flexible copper and tin coated copper wires of small thickness. The parameters were varied and the corresponding bond strength and structural changes were observed. There was a great breakthrough in their study which encompassed the removal of air bubbles and other undesired components present at the weldment. Amanat et al. [7] provided details pertaining to thermo plastic polymer welding for medical applications. Tests were conducted based on standards and codes. Heinze et al. [8] developed and proposed the temperature field of a pulsed gas metal arc weld of structural steel S355J2+N (ASTM A572 Gr. 50) with a thickness of 5 mm is experimentally and numerically investigated. In the case of temperature field validation, volumetric Gauss and double-ellipsoid Goldak heat sources were applied.

In existing literature it may be observed that reports and discussions on various factors of ultrasonic welding of Cu-Cu alloys are inadequate. Hence in this study an attempt is made to investigate the mechanical, metallographic and thermal aspects using experimental and computational techniques.

3. Experimentation

3.1 Materials for experimentation. The copper alloy C11000C (Cu-ETP) is used for this study and the chemical composition and physical properties of Cu-ETP material are provided below (Tables 1 and 2).

Table 1
Chemical composition of Cu-ETP

Cu (%)	O (%)
Min 99.90	Max 0.04

C11000C electrolytic tough pitch copper (ETP), an electrolytic refined copper widely demanded for its deployment in electrical and electronic applications, is being investigated for its weld-ability in this study. Cu-ETP possesses properties necessary in all applications with a hydrogen-free ambience. In the presence of H₂ and heat all oxygen-bearing coppers suffer from so-called hydrogen embrittlement (9). This is a chemical reduction of copper oxide by diffusing hydrogen leading

to formation of H₂O within the microstructure, resulting in embrittlement of the grain boundaries. The phosphorus of our copper content is very low, so that electrical conductivity is comparable to the best performing materials. C1100 is an oxygen containing copper which has a very high electrical and thermal conductivity. It has excellent forming properties. Due to its oxygen content soldering and welding properties are limited. Hence, this study attempts to address these weld ability issues of Cu-ETP with the employment of ultrasonic joining technique.

3.2 Experimental trials. The experimental studies are carried out for Cu-Cu alloy similar material welding. The reason attributed to the choice of these materials in particular is its demand in automobile and other manufacturing industries.

These materials are joined together (bonding) by employing ultrasonic welding machine [UWM M1000]. This machine is capable of delivering a power rating of 10 kW. This enables the variation of following variables that alters the property of the weldment decide the quality of weldment in terms of its integrity namely pressure, vibration etc. Figure 1 shows the machine used for this investigation. Trails were carried out by varying certain parameters while maintaining a constant value for the remaining parameters.

The range of the parameter (Table 3) is chosen from the survey carried out in the available literatures. The parameter that has insignificant influence on the weldment has been maintained constant. 20 trails are carried out for extensively analysing the weldments and to frame an optimum parameter window. Table 4 provides the details of the trails conducted for these experimental examinations.

Table 3
Levels of parameters

Pressure (bar)	Welding time (sec)	Amplitude (μm)
2.0	4	28
3.0	4.5	42
4.0	5	57

Pressure, welding time and amplitude have been set with 3 levels for the experimental trials while the frequency is maintained constant at 10 KHz.

It may be observed from Table 4 that as the pressure increases the quality of weldment improves. Subsequently the weldments are subjected to various tests to evaluate the

Table 2
Physical properties of Cu-ETP

Melting Point [°C]	Density [g/cm ³]	Specific Heat Cap at 20°C [kJ/kgK]	Electrical Conductivity [MS/m]	Thermal Conductivity at 20°C	Modulus of Elasticity [Gpa]	Co-efficient of Therm Exp at 20°C [10 ⁶ /K]
1083	8.94	0.394	58	390	127	17.7

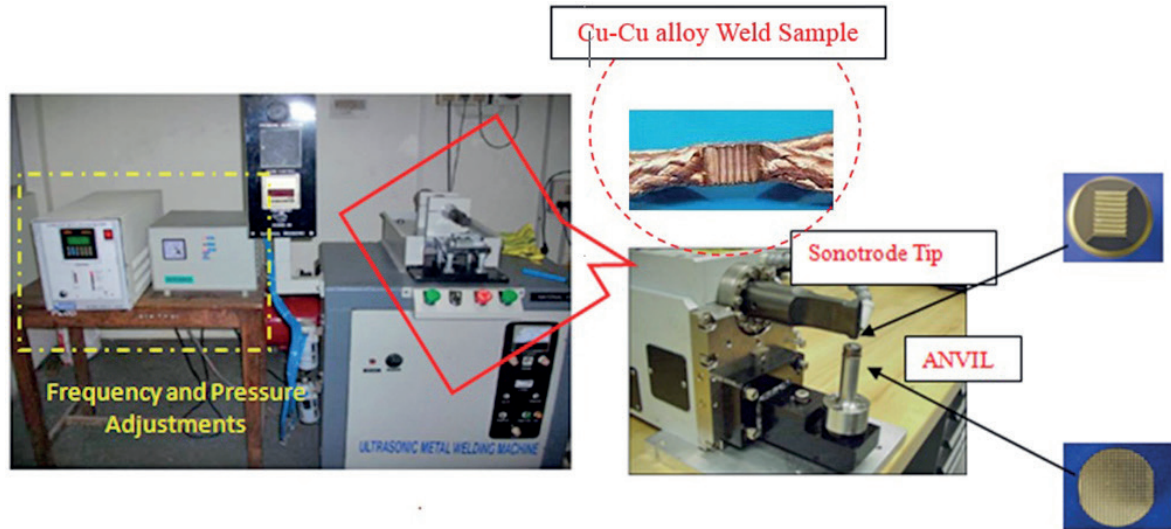


Fig. 1. Ultrasonic equipment

strength and quality. The tests are mainly carried out from the insight of global disciplines namely mechanical and metallurgical aspects.

Table 4
Weld strength for different trials

Exp. No	Pressure (bar)	Welding time (s)	Amplitude (μm)	Weld strength (Mpa)
1	2	5	28	261.20
2	2	4	28	256.35
3	3	4.5	42	318.19
4	3	4.5	57	320.45
5	4	4.5	42	430.39
6	4	5	57	446.82
7	3	4.5	42	320.49
8	2	4.5	42	272.15
9	4	5	28	429.17
10	3	4.5	42	324.76
11	4	4	57	438.15
12	3	4.5	42	324.86
13	3	4.5	42	329.18
14	2	5	57	268.64
15	3	4	42	319.15
16	3	4.5	28	315.82
17	2	4	57	261.75
18	3	5	42	325.41
19	3	4.5	42	321.86
20	4	4	28	322.46

Destructive testing such as tensile strength analysis and hardness have been carried out. Further micro, macro and SEM pictures are captured to analyse the integrity of bonding. Paral-

lely, X-ray diffraction and EDAX are employed for determining the possibility of formation of intermetallics at the weldments. Besides, radiography is also employed to access the availability of pores or cluster of pores at the weldment. The observations are recorded and the inferences are derived which are presented in the following section.

4. Results and discussion

The similar wire welded Cu-ETP is shown in Figure 2.

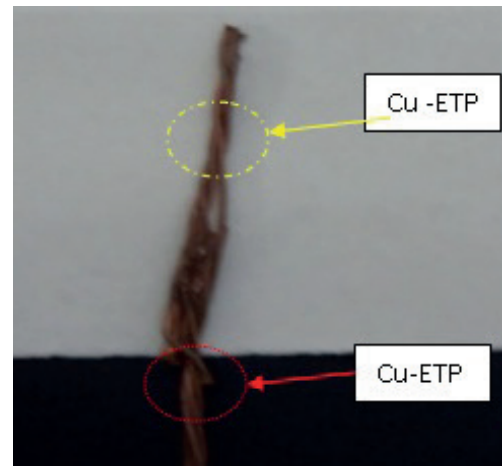


Fig. 2. Cu-ETP welded specimens

Samples welded with varying parameters are presented as shown in Fig. 2.

The interference drawn from the material testing of samples for all the trails is presented in Table 2. It may be clearly observed that some samples have achieved good bonding in terms of weld strength while the others appear to show lesser bond strength. This study discusses the tests carried out on specimens with good bonding strength. Destructive and Non-destructive

test along with the metallurgical characterization have been carried out to determine the causes underlying the achievement of good and faulty weldments.

4.1. Destructive testing of welded specimens.

4.1.1. Shear test. As part of destructive tests, shear test is performed to record the maximum load bearing capacity which is presented in Table 5. Almost all the welded specimens are well within the acceptable range. Fractures are noticed in few specimens analyzed using SEM. Tests are carried out for the base material and the welded specimens (Cu-Cu alloys).

Table 5
Shear test result for copper

S. No	TYPE OF MATERIAL	PRESSURE (bar)	WELD STRENGTH/ MAX LOAD WITHSTAND CAPACITY (MPa)
1.	Copper (ETP)	1.5	177.74 (joint with fracture)
2.		2.0	261.20
3.		2.5	281.17
4.		3.0	318.19
5.		3.5	376.39

4.1.2. Hardness test. Hardness of Cu metal wire of 1mm is measured by micro-vickers hardness machine on the weld and near the weld region. Slight decrease in the hardness can be noted adjacent to the welded surface caused by temperature rise during the welding process. The maximum load that it could with stand without getting broken was 93.1 and this gradually increased with increasing pressure up to 376.39 for copper, 73.2 to 93.1 for copper-copper weldments (Table 6).

Table 6
Hardness test results

Hardness test method : IS 1501-2002[Reaff – 2007]			
Sl No	Metal	Region	Hardness Value (HV)
1	Copper (ETP)	Base	70.4, 74.7, 69.4, 71.8, 65.4
2	Copper + Copper (ETP)	Base + HAZ Weld M	71.2, 64.9, 74.7, 69.3, 73.5 89.9, 93.1, 83.4, 78.4, 73.3



Fig. 3. Radiography pattern for welded joints

4.2. Non destructive testing. NDT needs to be used for any phase of a product's design and manufacturing process, including materials selection, research and development, assembly, quality control and maintenance. Radiographic testing is one of the oldest methods of non-destructive testing and has been in use for approximately five decades. Radiography using X-rays is one of the NDT techniques used for imaging the joints to detect and locate defects. In the present study, Aluminium joints are evaluated by radiographic inspection; Fig. 3 is an example of the radiographic patterns for weld joint.

The quality of ultrasonic welded specimens is assessed using non-destructive testing. Radiography using X-ray is employed to identify and analyse the defects at the ultrasonic welded joint. From the results it is observed that there are no pores or cluster of pores either in the weld region or in the vicinity.

Thus this study, demonstrates that the weld is free from impurities and other gas molecules. Eventually this fact leads to greater integrity in the weldment and shows the reliability of the process.

4.3. Metallurgical characterization.

4.3.1. Macro structural studies. The macrographs for Cu ETP alloy welds are presented in figure 4 respectively. The weld is distinct with solidification lines clearly visible. The centre line mark indicates the fused mass of materials.

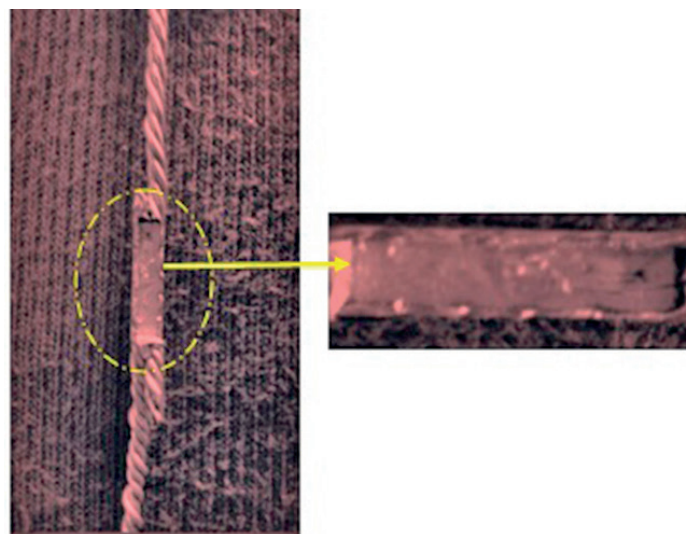


Fig. 4. Macrostructure of CuETP wire weld

No pores or voids or cracks (indicates good quality of weld without impurities or gas)

4.3.2. Micro structural studies. From the micrographs (Fig. 5) it may be observed that no distinct fusion line or HAZ is visible. The weld region is merged with the HAZ owing to the fact that it encounters higher rate of instantaneous heating and subsequent higher rate of cooling. Microstructure (Fig. 5) depicts equated grains and annealing twins distributed in a matrix of copper throughout the structure.

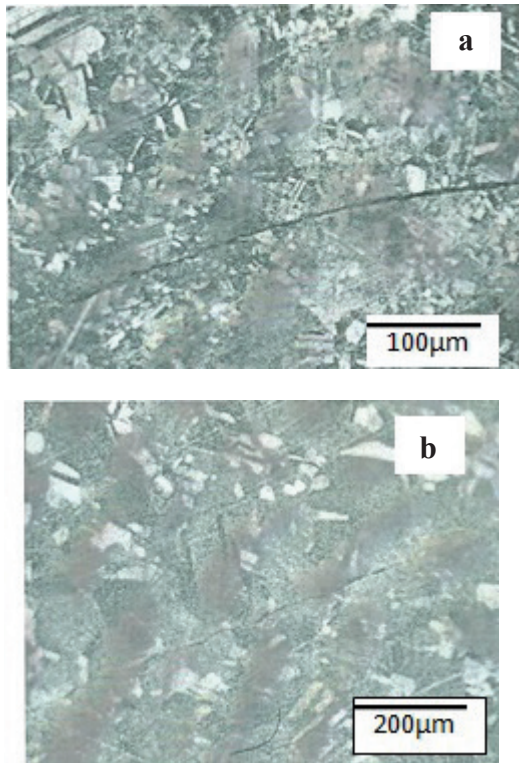


Fig. 5. Microstructural images of CuETP weld (LM)

4.3.3. SEM, EDAX results. The SEM image of the cross section of Cu weldments shows the formation of oxides between copper-copper weldments. From SEM images formation of oxides and its composition is observed through the graph. The microscopic examinations are conducted in order to observe the welding region, orientation of metal composites in the welding zone and the thickness of the weld. The fracture surfaces of selected samples are examined using SEM in order to assess the cracks in the weldments. The welded regions reveal the brighter areas which also confirm the formation of impurities.

Figure 6 shows EDX analysis of the points defined on the SEM microstructure at the interface region of the welded Cu -Cu joints. Figure 6 illustrates the EDX analysis results of point on the Cu side of the SEM micrographs. However, in this particular sample the grains have oozed out indicating non uniform bonding which may lead to cracks and failure. This may be owing to the fact that the pressure, or the time or the heat was insufficient which are prone to brittle fractures. However, he other aspects provide well enough evidence that strong joints can be produced by ultrasonic welding method.

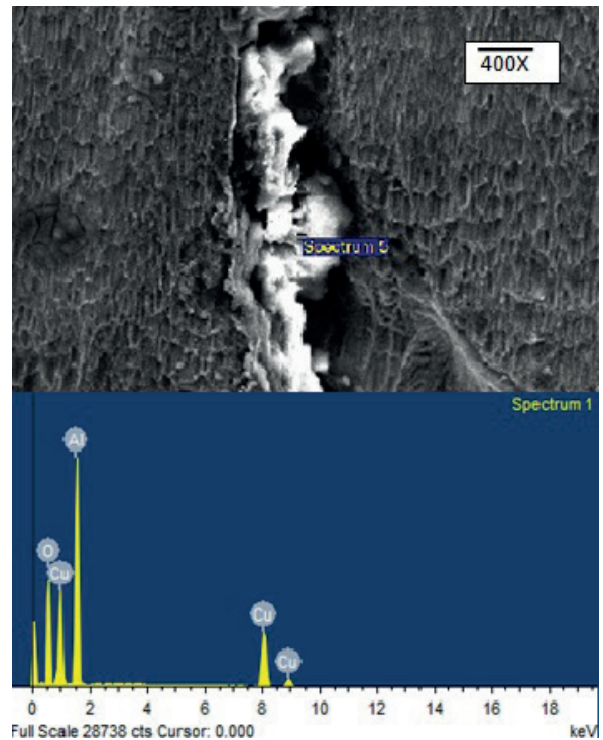


Fig. 6. SEM and EDAX of Cu-ETP weldment

4.3.4. XRD. X-ray diffraction patterns are obtained using Rigaku X – ray diffractometer with CuK α radiation ($\lambda = 1.5406 \text{ \AA}$) with 2θ ranging from 10° to 80° . Indexing of planes is done and the peaks are compared with the standard JCPDS (Joint Committee of Powder Diffraction Standards) values.

Figure 7 shows the X-ray diffraction patterns of the base metal and weld region respectively. The line broadening of the diffraction peaks arises due to the particle size and strain present inside material. The X-ray diffraction Spectra provides information on the crystal phase in the base metal. The tallest peak contains Cu in a cubical phase. Similarly the other peaks constitute either cubical phase Cu. There are a few irregularities with no defined peaks indicating the existence of impurity phases. A good crystalline nature is observed in the base metal.

Similarly, The X-ray diffraction Spectra (Fig. 7) provides information on crystal phase in the weld region. The tallest peak contains Cu existing in a cubical phase. Similarly the other peaks constitute either hexagonal phase cubical phase Cu. The weld region retains the same chemical composition as that of the base metal indicating that there are no impurities formed in the weldment.

5. Response surface methodology for parametric analysis

Second order RSM based models are developed for mould strength to analyse the parametric interaction effects on pressure, welding time and amplitude by plotting 3D response surface plots. RSM facilitates in determining the optimum range of weld strength for an optimal input parametric combination of pressure, welding time and amplitude.

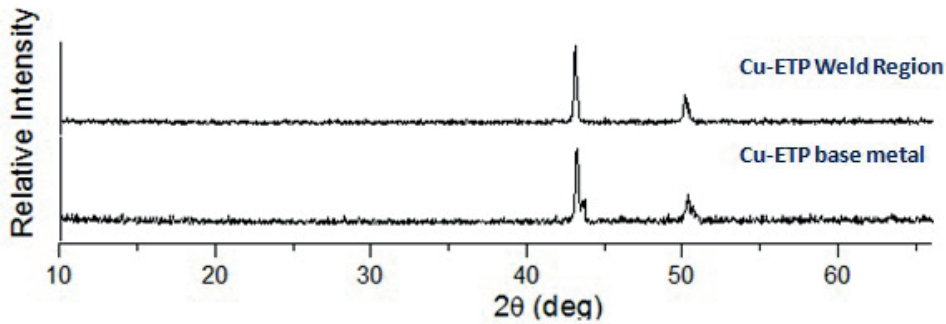


Fig. 7. XRD pattern for base metal and weld region

This implies that the models proposed are adequate and there is no reason to suspect any violation of the independence or constant variance assumption. Main effects plot is developed for the response variable for each level of a factor. The main effect is calculated by subtracting the overall mean for the factor from the mean for each level. Figure 8 shows locations of the main effects for input parameters and weld strength respectively and it emphasizes that pressure, welding time and amplitude factors increase when moved from the low level to the high level. Each level of the factors affects the response differently.

Each factor at their high level results in higher mean responses compared to that at the low level. Alternatively, the pressures appear to have a greater influence on the responses as compared with remaining slope.

The analysis of variance (ANOVA) technique [10] is employed to check the adequacy of the developed models at 95% confidence interval. As per the ANOVA technique, the model is adequate within the confidence level which indicates that calculated value of the F ratio, the lack of fit to the pure error does not exceed the standard tabulated value of F-ratio [11]. Here, pressure, welding time and amplitude models are adequate in non-linear form as illustrated in Table 7.

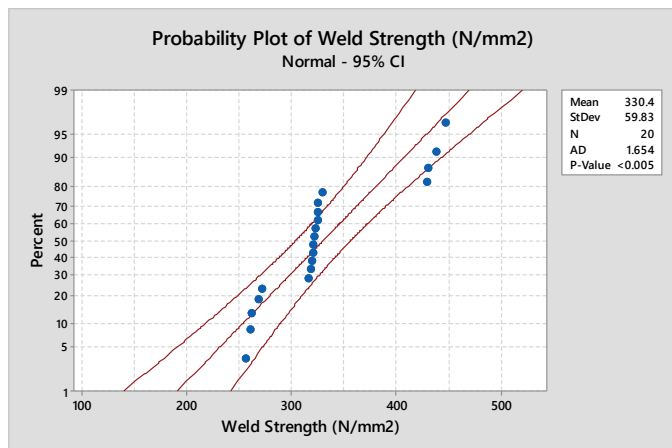


Fig. 8. Probability plot of weld strength

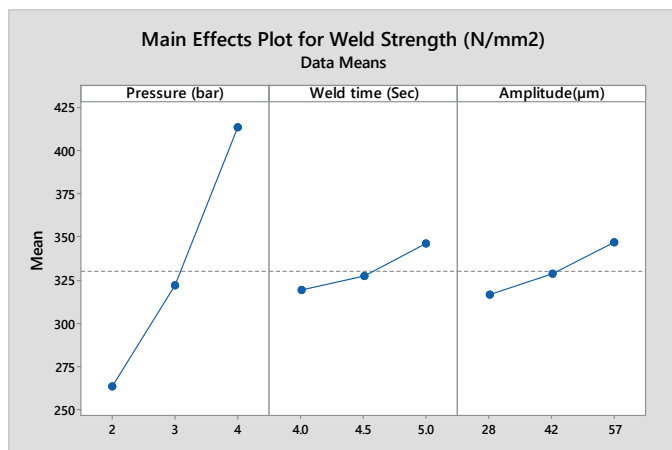


Fig. 9. Main effect plot for weld strength

Table 7
ANOVA analysis

Analysis of Variance					
Source	DF	Adj SS	Adj MS	F-Value	P-Value
Model	9	65908.0	7323.1	34.68	0.000
Linear	3	59968.9	19989.6	94.66	0.000
Pressure(bar)	1	55937.5	55937.5	264.89	0.000
Welding time (s)	1	1757.1	1757.1	8.32	0.016
Amplitude (µm)	1	2274.4	2274.4	10.77	0.008
Square	3	1769.1	589.7	2.79	0.095
Pressure (bar)	1	1654.7	1654.7	7.84	0.019
Welding time (s)	1	54.7	54.7	0.26	0.622
Amplitude (µm)	1	228.9	228.9	1.08	0.322
2-Way Interaction	3	4283.0	1427.7	6.76	0.009
Pressure (bar). Welding time (s)	1	1342.7	1342.7	6.36	0.030
Pressure (bar). Amplitude (µm)	1	1805.4	1805.4	8.55	0.015
Welding time (s). Amplitude (µm)	1	1134.9	1134.9	5.37	0.043
Error	10	2111.7	211.2		
Lack of Fit	5	2036.5	407.3	27.09	0.001
Pure error	5	75.2	15.0		
Total	19	68019.7			

Table 8
Coded coefficient values

Coded Coefficients						
Term	Effects	Coef	SE Coef	T- Value	P-Value	VIF
Constant		325.16	5.00	65.03	0.000	
Pressure (bar)	149.59	74.79	4.60	16.28	0.000	1.00
Welding time (s)	26.51	13.26	4.60	2.88	0.016	1.00
Amplitude (µm)	30.16	15.08	4.60	3.28	0.008	1.00
Pressure (bar). Pressure (bar)	49.06	24.53	8.76	2.80	0.019	1.82
Welding time (s). Welding time (s)	-8.92	-4.46	8.76	-0.51	0.622	1.82
Amplitude (µm)	-18.27	-9.14	8.77	-1.04	0.322	1.82
Pressure (bar). Welding time (s)	25.91	12.96	5.14	2.52	0.030	1.00
Pressure (bar). Amplitude (µm)	30.04	15.02	5.14	2.92	0.015	1.00
Welding time (s). Amplitude (µm)	-23.82	-11.91	5.14	-2.32	0.043	1.00

Regression equation

$$\begin{aligned}
 \text{Weld Strength (MPa)} = & -114 - 233.0 \text{ Pressure (bar)} + 179 \text{ Welding time (s)} \\
 & + 9.02 \text{ Amplitude (}\mu\text{m)} + 24.53 \text{ Pressure (bar)*Pressure (bar)} \\
 & - 17.8 \text{ Welding time (s)*Welding time (s)} \\
 & - 0.0435 \text{ Amplitude (}\mu\text{m)*Amplitude (}\mu\text{m)} \\
 & + 25.9 \text{ Pressure (bar)*Welding time (s)} \\
 & + 1.036 \text{ Pressure (bar)*Amplitude (}\mu\text{m)} \\
 & - 1.643 \text{ Welding time (s)*Amplitude (}\mu\text{m)} \quad (1)
 \end{aligned}$$

It is imperative to perform test for significance of the regression model, test for significance on individual model coefficients and test for lack-of-fit need to be performed. Table 5 shows the ANOVA table for response surface model for weld strength. The value of “F” in Table 5 for model is less than 0.05 which conveys that the model is significant, which is desirable as it indicates that the terms in the model have a significant effect on the response. In the same manner, the main effect of pressure (bar) and welding time(s), the two-level interaction pressure *welding time, welding time * amplitude and pressure * amplitude are significant model terms. Other model terms are insignificant. These insignificant model terms (not counting those required to support hierarchy) may be eliminated to obtain an improved model. The lack-of-fit can also be insignificant. The main effect of pressure and welding time is the most significant factor associated with welding of Cu/Cu alloys weldments. Results from Table 8 show that the coefficient of determination is also used to test the goodness-of-weld of the pressure and welding time, which provides a measure of variability in the observed response values and may be explained by the controllable factors and their interactions.

Table 9
Fits and diagnostic observations

Observation	Weld Strength (MPa)	Fit	Resid	Std Resid
14	269	249.75	18.89	2.88 R
20	322	342.67	-20.21	-3.03 R

While comparing the predicted values of strength with experimental values, it is observed that the deviations are minimal except for a few combinations of parameters. The average of deviation (%) between theoretical weld strength and experimental weld strength for ultrasonic welded joints of Cu-ETA blends are minimal. The optimum weld strength obtained from experiments and RSM for Cu-ETA blend are shown in Table 9.

The surface plot graph is helpful to see the shape of a response surface; hills, valleys, and ridge lines. Hence, Eq. (2) function $f(p, a)$ can be plotted versus the levels of p and a as

shown as Fig. 10. In this graph, each value of p and a generates a y -value. This three-dimensional graph shows the response surface from the side. The contour plots Fig. 11 are produced using (1), the calculated fitted coefficient and by holding one of the variables constant are shown as “hold values” in Fig. 11. The contour plot shows the weld strength as a result of amplitude and pressure. Weld strength increase while moving along the pressure axis and against the amplitude axis. ANOVA table depict that the pressure values are significant; nevertheless, the role of amplitude is insignificant. The curve (Fig. 12) represents the weld strength at different amplitude and different pressure ranges. Moreover, the slope of weld strength with respect to pressure values show changes of amplitude.

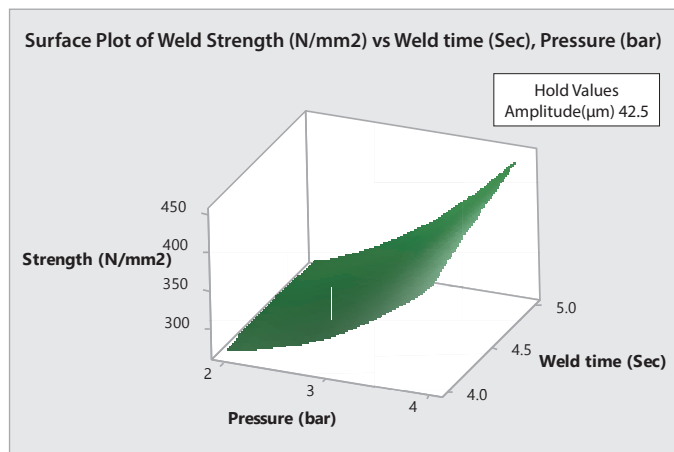


Fig. 10. Surface plot of weld strength vs. welding time, pressure

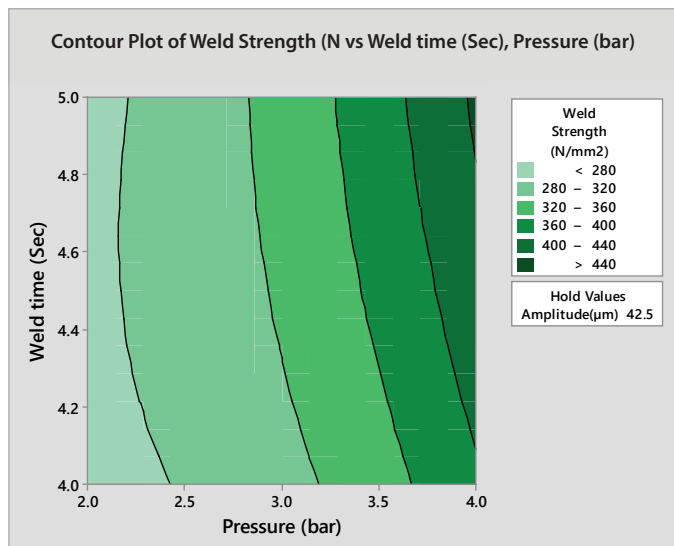


Fig. 11. Contour plot of weld strength Vs Welding time, Pressure

From (1), function $f(p, t)$ can be plotted versus the levels of p and t as shown as Fig. 12. Surface plot of weld strength Vs pressure and welding time, this “hold value” in Fig. 12. From this plot pressure and welding time are contribute more to the weld strength. The calculated fitted coefficient and by holding

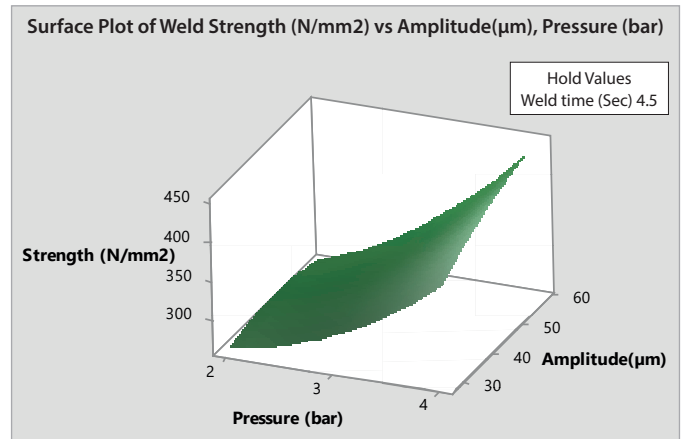


Fig. 12. Surface plot of weld strength vs. amplitude, pressure

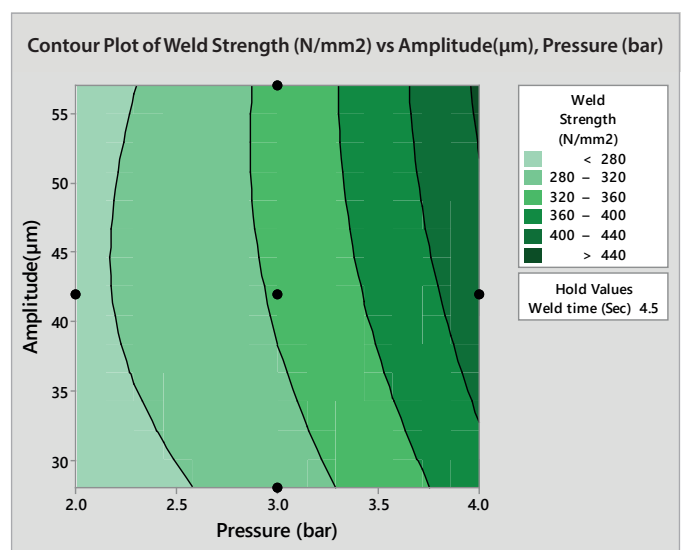


Fig. 13. Contour plot of weld strength vs. amplitude, pressure

one of the variables constant are shown as “hold values” in Fig. 13. The contour plot shows the significant different in weld strength as a result of pressure and welding time. This is clearly observed from increasing weld strength while moving along the pressure axis as well as the welding time axis. The observation is similar to the previously repeated results.

From (1), function $f(t, a)$ is plotted for the levels of t and a as shown as Fig. 14. In this graph, each value of t and a , generates a y -value. Surface plot “hold value” is shown in Fig. 14, which shows that weld strength is affected meagrely when compared with other plots. The weld strength is not affected by these values as only small changes occur. The coefficient is fitted by holding one of the variables constant are shown as “hold values” in Fig. 15. The contour plot shows the significant difference in weld strength as a result of amplitude and welding time. It is observed that there is an increase in the weld strength while moving along the amplitude axis from the overall analysis, it may be emphasized that the contribution shown by pressure is higher. The curve representing weld strength at different amplitude and different welding time ranges are also discussed.

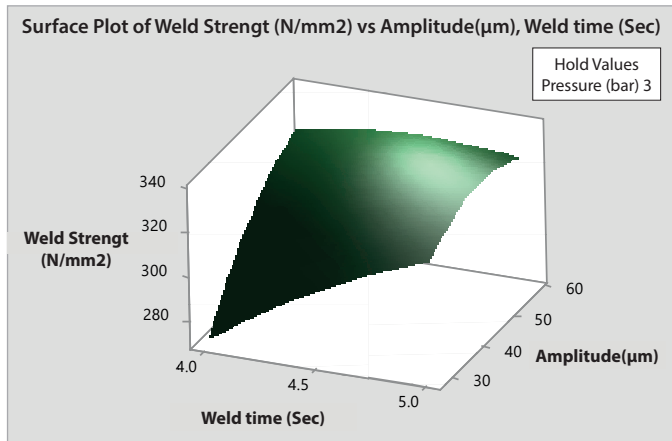


Fig. 14. Surface plot of weld strength vs. amplitude, welding time

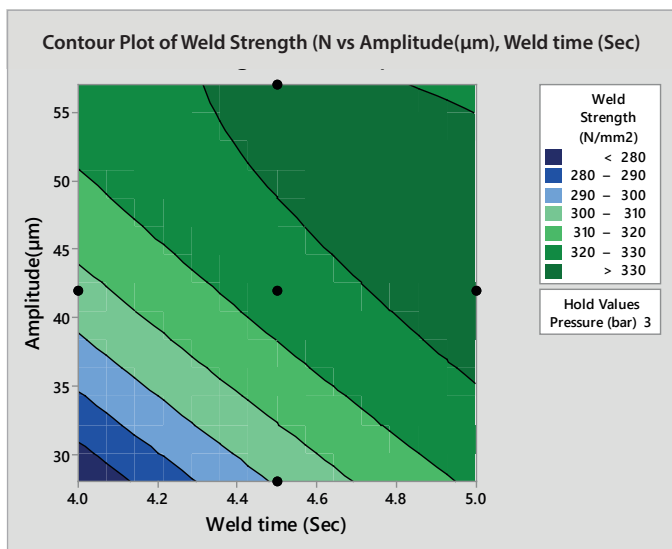


Fig. 15. Contour plot of weld strength vs. amplitude, welding time

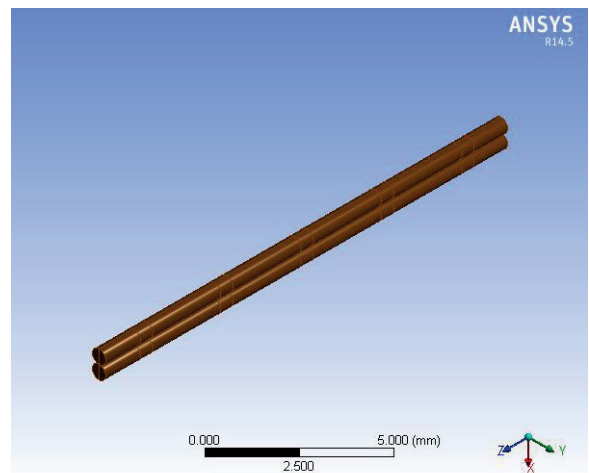
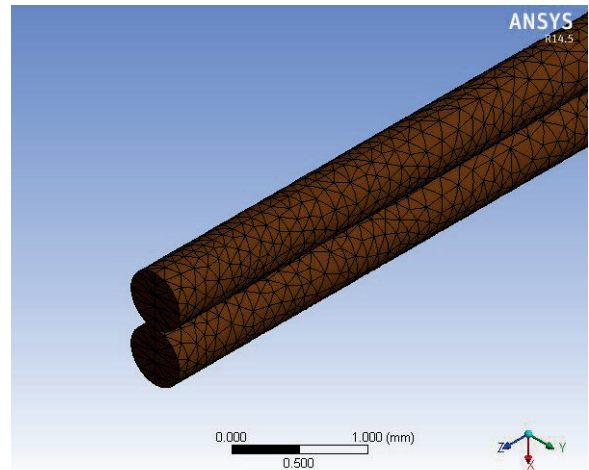


Fig. 16. FEM model for thermal analysis with meshing

6. Thermal analysis in ultrasonic welding process

A non-linear transient thermal analysis is performed for ultrasonic welding process to predict the temperature history of the domain for complete thermal cycle multi pass welding along the thickness. Computer based simulations offer the possibility to examine different aspects of the process without having a physical prototype of the product. In this work, main parameters of the ultrasonic welding process are considered and the finite element simulation is performed using ANSYS.

6.1. Mathematical model for heat transfer simulation in ultrasonic welding process. The heat transfer in the base material is conceived to be three dimensional models in nature considering the radial, circumferential and axial directions [12]. Figure 16 shows the three dimensional model which typically depicts the butt joint configuration with the associated boundary conditions being incorporated. Figure 16 shows the FEM model of Al wires being welded and the triangular meshing adopted for this study.

Welding simulation procedure is depicted in Fig. 17.

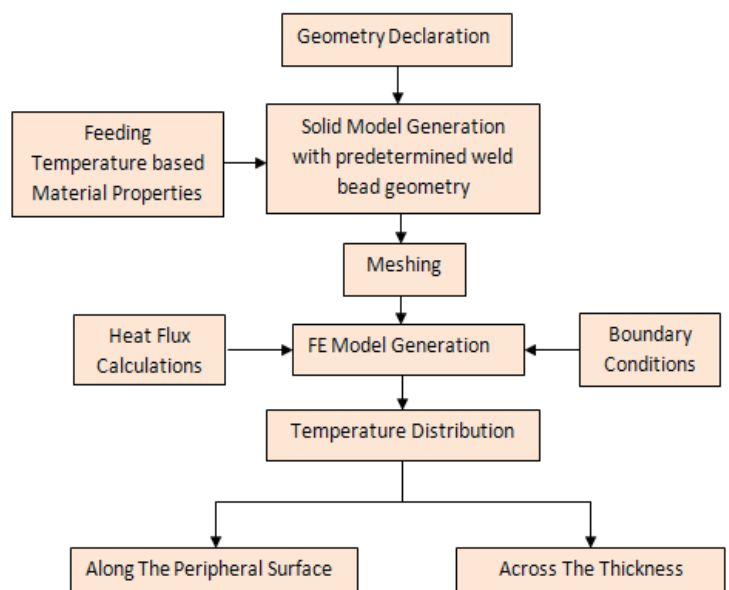


Fig. 17. Steps followed in FEM analysis

The dimensions of all the specimens considered for this study is 0.3 mm. The length of each specimen is approximately 50 mm. The input parameter for the three-dimensional model is chosen as per the trial of Table 1 as it yielded a full penetration and good weld. The length used for the calculation by FEM is 50 mm, because the heat affected zone of ultrasonic welded joint is very short. A free mesh is adopted for the calculation which includes a total of 56,760 nodes and 16,589 elements for the calculation domain as shown in Fig. 16. The calculation domain is increased and selected through a series of calculations for this size, which shows a uniform distribution of heat flux.

6.1.1. Material properties. The material used for the study is Cu-ETP. Material properties, namely thermal and mechanical properties of the joint for Cu-Cu material are used for the numerical analysis.

6.1.2. Boundary condition and heat input. For this study, an assumption is made that the ultrasonic welding process is carried out at room temperature with air as the medium in the set up. The necessary mathematical equations for the FEA are adopted here.

6.2. Heat generation during ultrasonic welding. The ultrasonic mechanical energy, subsequently converted to thermal energy, can be determined by the local cyclic stress (x), strain (y), friction shear (z), and component slip (ex) at the interface surface. Heat is generated (a) locally in the control volume, ($Q_v(x,y, z)$), by inelastic hysteresis and plastic deformation, and (b) at the interface surfaces, ($Q_s(x, y)$), by friction, during each cycle at the ultrasonic frequency, f.

$$Q_v(x, y, z) = f \oint \sigma_{eq}(\epsilon) d\epsilon_{eq} \quad (2)$$

$$Q_s(x, y) = f \oint \tau_x(\epsilon_x) d\epsilon_x = N \oint \mu \sigma_z(\epsilon_x) d\epsilon_x \quad (3)$$

Where σ_{eq} and ϵ_{eq} are equivalent stress and strain, and σ_z is normal compressive stress.

It is restricted tried to embed the plastic work in the numerical thermo mechanical coupled analysis of UW and quantitatively study the role of plastic work in ultrasonic bond formation. The above equations for calculating heat generation assume the mechanical state as a function of location only, not considering time and temperature influences. This thesis proposed a new method of calculating the plastic work, which uses the plastic work rate (\dot{W}^{pl}), proportional to the plastic strain rate, to account for the effects of location, temperature and time in ultrasonic welding.

$$\dot{W}^{pl}(x, y, z, t, T) = \sigma_j(x, y, z, t, T) \cdot \dot{\epsilon}_j^{pl}(x, y, z, t, T) \quad (4)$$

Where $j = 1, 2, 3$. It is assumed that some of the plastic work converts to heat, while the rest is stored as energy of crystal defects accompanying plastic deformation

6.3. Results and discussion. With the above mentioned numerical model, temperature distribution during MIAB welding is predicted and is illustrated in Fig. 18. It shows the thermal distribution at one cross section of the weld reinforcement. The hottest zone exists at 749 min exists on the centre of the weld reinforcement. A very high temperature gradient is observed near the weld line. Moreover, higher temperature and heat rate

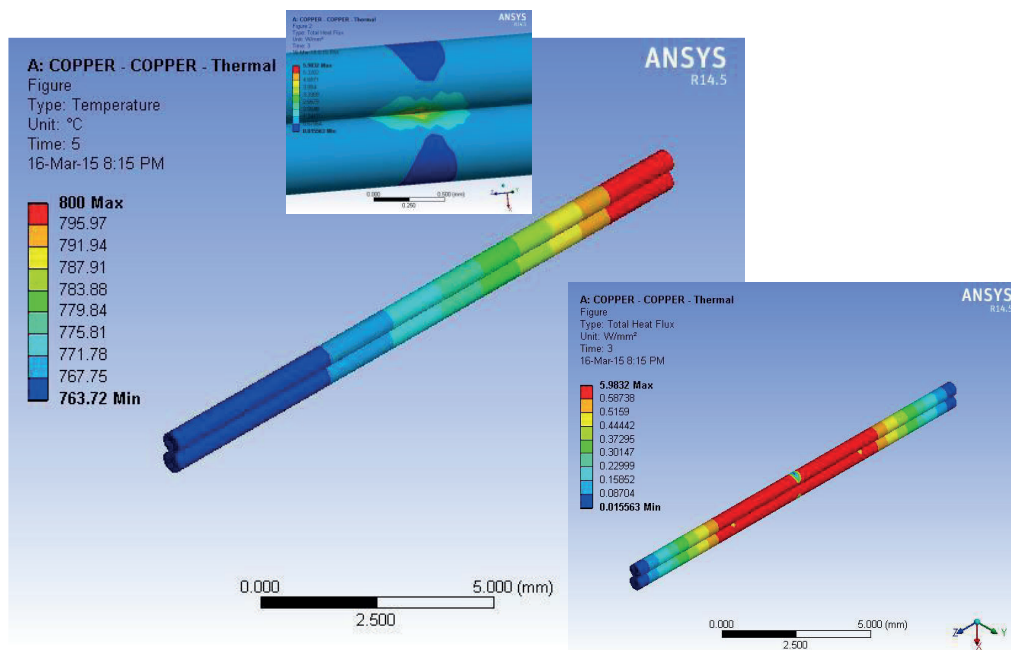


Fig. 18. Temperature distributions during ultrasonic welding process as indicated by FEA

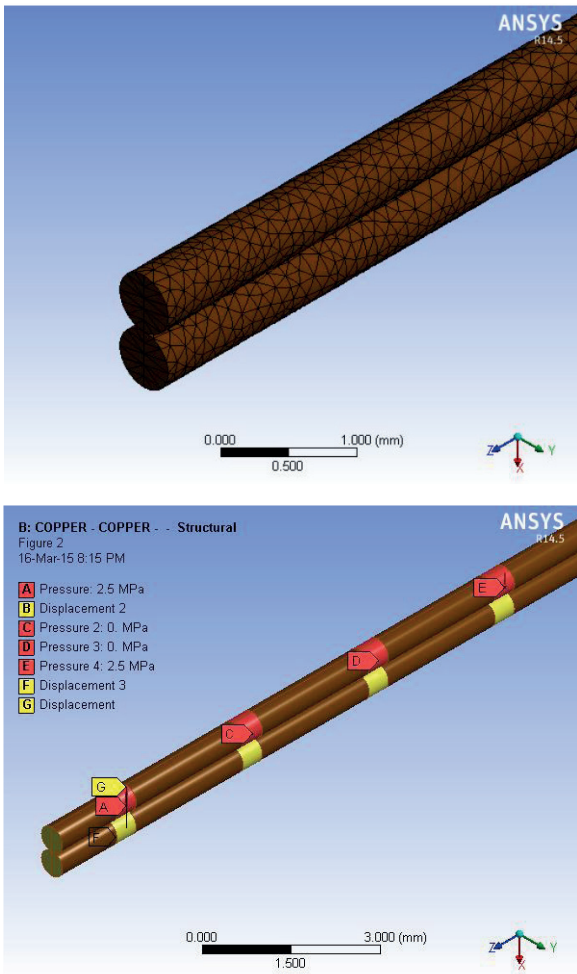


Fig. 19. Cu-ETP structural analysis with loading using FEM

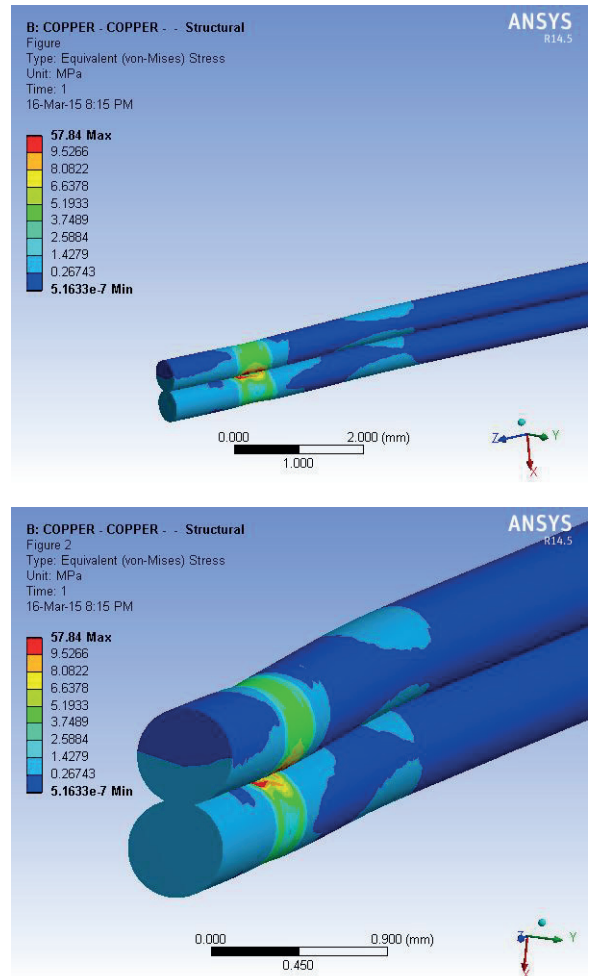


Fig. 20. Deformation and stress induced in the material during welding

are indicated nearer to the weld line. The temperature gradually decreases with increasing distance from the centre line of the weld reinforcement towards the parent metal.

Figure 19 clearly indicates the point at which load is applied and the pressure ranges of the horn that presses against the work piece. The displacement of the horn is also limited to 3 mm.

Expansion and deformation occurs steadily following the heating of Cu. Thermal stress is induced by the difference of lattice constants between the dissimilar particles. Figure (20) emphasizes that the thermal expansion induced the tensile stress at Cu near the weld interface.

7. Validation

The temperature at various portions of the specimens during the Cu-Cu alloy welding using ultrasonic joining process is recorded with the help of infrared guns. The results obtained from FEM analysis is compared with the experimental result in Fig. 21. It is observed that, there is a good coherence between the simulated and experimental results proving the validity of the FEM model. Small deviations of the FEM results compared

to the experimental recordings observed in Fig. 21 are due to the physical conditions altering the measurement during experimentation.

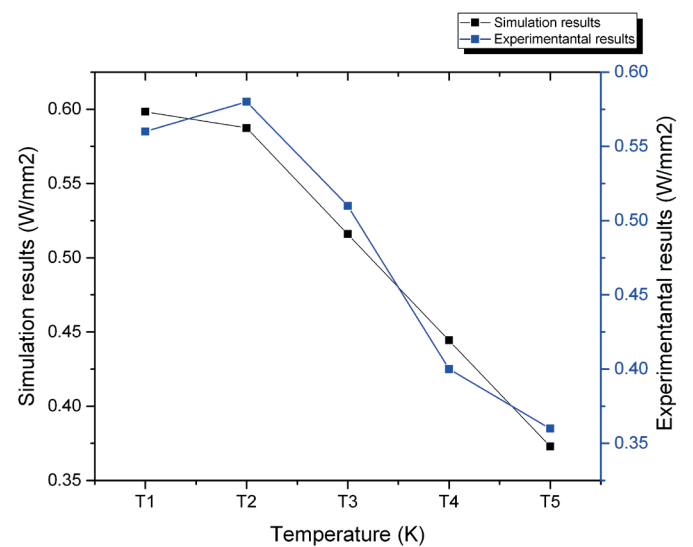


Fig. 21. Temperature distributions for simulated and experimental results

8. Conclusions

Metallurgical characterizations, destructive and non-destructive tests are carried out on ultrasonic welded Cu-Cu joints. Further, FEM analysis is performed to determine the temperature distribution. Significant conclusions from these tests are summarized as follows:

1. The strength and quality of ultrasonic welded joints are in the acceptable range.
2. Macro and Micro structural analysis illustrates good bonding and integrity.
3. The faults have been identified using SEM which demonstrates irregularities and improper bonding in certain specimens owing to either low pressure, low heat are insufficient vibrations. On and overview it may be emphasize the joining non-ferrous materials using ultrasonics is more feasible.
4. The FEM results show good coherence with the experimental findings. It gives an insight into the deformation and the corresponding stress induced in the material following the ultrasonic welding process.

REFERENCES

- [1] J. Tsujino and T. Ueoko, "Ultrasonic butt welding of aluminum, anticorrosive aluminum and copper plate specimens", *Ultrasonics Symposium*, 493–496 (1988).
- [2] J. Tsujino, T. Ueoko, Y. Suzaki, K. Uchida, I. Watanabe, and A. Anodh, "Ultrasonic butt welding of thick metal plate specimens using a large capacity static induction thyristor power amplifier", *Ultrasonics Symposium*, 371–374 (1990).
- [3] J. Tsujino, T. Ueoko, I. Watanabe, Y. Kimura, T. Mori, K. Hasegawa, Y. Fujita, T. Shiraki, and M. Motonaga, "New methods of ultrasonic metal welding", *Ultrasonics Symposium*, 405–410 (1993).
- [4] J. Kim, B. Jeong, M. Chiao, and L. Lin, "Ultrasonic bonding for MEMS sealing and packaging", *IEEE Transactions on Advanced Packaging*, 2 (32), 461–467 (2009).
- [5] J. Tsujino, T. Murakoshi and E. Sugimoto, "Welding characteristics of aluminum, copper, nickel and aluminum alloy with alumina coating using ultrasonic with alumina coating using ultrasonic complex vibration welding equipment", *IEEE International Ultrasonics Symposium*, 1211–1214 (2009).
- [6] J. Tsujino, T. Yokozula, S. Suga, and E. Sugimoto, "Welding characteristics of bi-metal, braided wires, aluminum and copper foils using 20 KHZ ultrasonic complex vibration welding equipment", *IEEE International Ultrasonics Symposium*, 1420–1423 (2010).
- [7] N. Amanat, N.L. James, and D.R. McKenzie, "Welding methods for joining thermoplastic polymers for the hermetic enclosure of medical devices", *Medical Engineering & Physics*, 690–699 (2010).
- [8] C. Heinze, C. Schwenk, and M. Rethmeier, "Effect of heat source configuration on the result quality of numerical calculation of welding-induced distortion", *Simulation Modelling Practice and Theory*, 1 (20), 112–123 (2012).
- [9] J.R. Davis, *ASM Specialty Handbook, Copper and Copper Alloys*, ASM International, Metals Park, 2010.
- [10] W. G. Cochran and G. M. Cox, *Lattice Designs and Experimental Designs*, John Wiley & Sons, New York (1992).
- [11] V.N. Gaitonde et al., "Genetic algorithm-based burr size minimization in drilling of AISI 316L stainless steel", *Journal of Materials Processing Technology*, 1(197), 225–236 (2008).
- [12] G. Padmanaban and V. Balasubramanian, "Optimization of laser beam welding process parameters to attain maximum tensile strength in AZ31B magnesium alloy", *Journal of Optics & Laser Technology*, 2(42), 1253–1260 (2010).